

Cite this: *Chem. Sci.*, 2025, 16, 16225

All publication charges for this article have been paid for by the Royal Society of Chemistry

# A scalable zinc-based coordination network for energy-efficient NF<sub>3</sub>/CF<sub>4</sub> separation with unprecedented selectivity

Yi-Tao Li,<sup>†a</sup> Weilin Li,<sup>†b</sup> Li-Ping Zhang,<sup>a</sup> Na Geng,<sup>c</sup> Li Xu,<sup>a</sup> Shao-Min Wang,<sup>a</sup> Tingyu Zhu,<sup>c</sup> Qingqing Guan,<sup>\*d</sup> Yangyang Guo,<sup>\*c</sup> Xingxing Li<sup>†b</sup> <sup>\*a</sup> and Qing-Yuan Yang<sup>†b</sup> <sup>\*a</sup>

Nitrogen trifluoride (NF<sub>3</sub>) and carbon tetrafluoride (CF<sub>4</sub>) are critical gases in the semiconductor industry. However, their current lack of effective recycling and separation results in significant waste emissions, which are not only costly but also pose significant environmental challenges. Their separation remains a critical challenge due to their nearly identical physicochemical properties ( $\Delta bp < 1$  °C, similar polarizability). Here, we demonstrate that a zinc-based metal–organic framework (CALF-20) with precisely tuned 4.8 Å pores achieves exceptional NF<sub>3</sub>/CF<sub>4</sub> separation through molecular sieving. At 298 K, this material exhibits a record-high NF<sub>3</sub>/CF<sub>4</sub> adsorption ratio of 41.1, and a CF<sub>4</sub> purity of 99.5% can be achieved through breakthrough experiments. Structural characterization and computational studies reveal that the unique pore channel properties preferentially adsorb NF<sub>3</sub> (kinetic diameter: 4.5 Å) while effectively excluding CF<sub>4</sub> (4.8 Å). This advance enables cost-effective gas purification at \$12.3 per kilogram, providing a practical solution for sustainable semiconductor manufacturing.

Received 5th July 2025  
Accepted 5th August 2025

DOI: 10.1039/d5sc04966k

rsc.li/chemical-science

## Introduction

Following a decade of advancement, the global semiconductor market is projected to attain a valuation of one trillion dollars by the year 2030.<sup>1</sup> Fluorinated electronic specialty gases, including NF<sub>3</sub>, CF<sub>4</sub> and other fluorinated gases, play an essential role in contemporary semiconductor manufacturing due to their distinctive chemical reactivity during plasma etching and cleaning processes.<sup>2,3</sup> However, the semiconductor industry, which serves as a fundamental component of the global digital economy, is confronted with a growing environmental dilemma. The fluorinated process gases critical to semiconductor manufacturing – nitrogen trifluoride (NF<sub>3</sub>) and carbon tetrafluoride (CF<sub>4</sub>) – exhibit extraordinarily high global warming potentials (GWPs) of 17 200 and 6500 CO<sub>2</sub>-equivalent,

respectively, with atmospheric lifetimes of 740 years for NF<sub>3</sub> and 50 000 years for CF<sub>4</sub>.<sup>4,5</sup> In the semiconductor manufacturing process, only a small portion of fluorinated gases are fully utilized, and a large amount of CF<sub>4</sub> and NF<sub>3</sub> exhaust gases remain stable after etching and cleaning, requiring high-temperature combustion or thermal plasma decomposition to effectively remove them.<sup>6</sup> Despite the treatment of exhaust gases, these trace amounts of fluorine-containing compounds inevitably escape into the atmosphere through ventilation systems.<sup>7</sup> The emissions of fluorinated gases from the global semiconductor industry are experiencing a year-on-year increase, which poses a considerable threat to the environment.<sup>8,9</sup> The separation and recycling of NF<sub>3</sub> and CF<sub>4</sub> through advanced separation technologies not only enable their efficient recovery for industrial reuse—significantly reducing operational costs—but also promote optimal resource utilization. Importantly, this approach significantly mitigates F-gas emissions, substantially diminishing their environmental impact.

Current industrial recovery of fluorinated gases predominantly relies on cryogenic distillation and liquefaction techniques, which operate under energetically demanding high-pressure and low-temperature conditions.<sup>10,11</sup> Porous adsorbent-based separation has emerged as an energy-efficient and economically viable strategy for the enrichment and recovery of high-value specialty gases. Porous materials—including zeolites,<sup>12</sup> activated carbons,<sup>13–15</sup> metal–organic frameworks (MOFs),<sup>16,17</sup> and porous organic cages—have demonstrated potential for fluorinated gas (F-gas) separation.

<sup>a</sup>State Key Laboratory of Fluorine & Nitrogen Chemicals, National Innovation Platform (Center) for Industry-Education Integration of Energy Storage Technology, School of Chemical Engineering and Technology, Xi'an Jiaotong University, Xi'an, 710049, China. E-mail: qingyuan.yang@xjtu.edu.cn

<sup>b</sup>Hefei National Research Center for Physical Sciences at the Microscale, University of Science and Technology of China, Anhui, 230026, China. E-mail: lixx@ustc.edu.cn

<sup>c</sup>CAS Key Laboratory of Green Process and Engineering, Institute of Process Engineering, Chinese Academy of Sciences, Beijing 100190, China. E-mail: yyguo@ipe.ac.cn

<sup>d</sup>Key Laboratory of Oil and Gas Fine Chemicals of Ministry of Education, College of Chemical Engineering, Xinjiang University, Urumqi 830017, China. E-mail: guanqq@xju.edu.cn

<sup>†</sup> Y. T. Li and W. L. Li contributed equally to this work.



However, while numerous traditional porous materials have been investigated for  $\text{NF}_3/\text{N}_2$  and  $\text{CF}_4/\text{N}_2$  separation, most reported adsorbents demonstrate limited selectivity for  $\text{NF}_3/\text{CF}_4$ . The separation of  $\text{NF}_3$  and  $\text{CF}_4$  remains a significant challenge in gas purification due to their nearly identical kinetic diameters. The urgency to address this challenge is further emphasized by the pledge of the semiconductor industry to achieve net-zero emissions by 2050.<sup>18</sup> This imperative demands the development of advanced materials that can effectively balance industrial scalability requirements with the need for molecular-level precision (Scheme 1).

MOFs have emerged as highly efficient adsorbents for gas separation, offering tunable pore geometries and chemical functionalities.<sup>19</sup> Recent advances in ultra-microporous MOFs (pore size <7 Å) demonstrate exceptional selectivity for fluorinated gases (F-gases) *via* size exclusion and host-guest interactions. For instance, amino-functionalized  $\text{NH}_2$ -Ni-MOF achieves a  $\text{CF}_4/\text{N}_2$  selectivity of 46.3 through optimized van der Waals interactions,<sup>20</sup> while Co-MOF-74 exhibits  $\text{NF}_3/\text{N}_2$  selectivity of 299.6 *via* Lewis acid-base interactions at open metal sites.<sup>21</sup> Although some MOF materials have exhibited favorable performance in separating specific fluorinated gases, no MOF material has currently achieved effective sieving of  $\text{NF}_3/\text{CF}_4$ . This is primarily due to the critical limitations inherent in MOF materials: (1) pore collapse during F-gas adsorption (*e.g.*, the M-MOF-74 series), whereas CALF-20 maintains high stability in both five cycles of static  $\text{NF}_3$  adsorption and dynamic breakthrough experiments; (2) the failure of previous adsorbents to discriminate between  $\text{NF}_3$  and  $\text{CF}_4$  during adsorption processes, in contrast to CALF-20, which exhibits a record-high  $\text{NF}_3/\text{CF}_4$  adsorption ratio of 41.1; (3) synthetic complexity that hinders scale-up, while CALF-20 is the first MOF material produced on an industrial scale. Achieving simultaneous high

selectivity, structural stability, and industrial viability remains a long-standing challenge.

Extensive research suggests that realizing efficient  $\text{NF}_3/\text{CF}_4$  separation necessitates MOF materials with meticulously tailored pore dimensions and the exclusion of open metal sites. These rigorous specifications substantially narrow the scope of candidate materials. When stability requirements and cost considerations are additionally factored in, CALF-20 emerges as the most promising viable option currently available. The separation of  $\text{NF}_3$  and  $\text{CF}_4$ , key fluorinated gases in semiconductor manufacturing, poses a significant challenge due to their similar kinetic diameters. Despite extensive research on MOFs as potential adsorbents for gas separation, achieving efficient  $\text{NF}_3/\text{CF}_4$  separation remains elusive. Existing MOF materials either lack the precise pore sizes required for molecular sieving or suffer from poor recyclability under industrial conditions, with many frameworks experiencing structural degradation after repeated adsorption cycles.

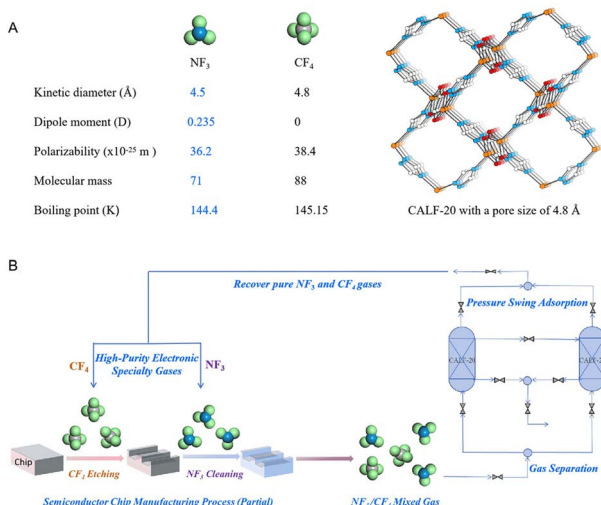
To address these limitations, this study focuses on developing scalable MOF adsorbents capable of molecular discrimination and practical recyclability for  $\text{NF}_3/\text{CF}_4$  separation. Herein, we introduce CALF-20, an industrially viable MOF engineered with precisely tuned 4.8 Å ultra-micropores. By utilizing steric exclusion effects, CALF-20 is designed to overcome the long-standing challenge of separating  $\text{NF}_3$  and  $\text{CF}_4$ . Notably, this material exhibits a record-high  $\text{NF}_3/\text{CF}_4$  selectivity of 41.1 and achieves >99.5%  $\text{CF}_4$  purity in breakthrough experiments.

This work not only proposes a material design strategy for targeted gas separation but also demonstrates the potential of CALF-20 in enabling the recovery of  $\text{NF}_3$  and  $\text{CF}_4$  through PSA systems. Such an approach offers a sustainable pathway for the energy-efficient recovery of fluorinated gases, in line with the goal of the semiconductor industry to achieve net-zero emissions by 2050.<sup>22</sup>

## Results and discussion

### Adsorption performance of CALF-20 for $\text{NF}_3$

CALF-20 is constructed from zinc(II) ion layers interconnected by 1,2,4-triazole ligands and oxalate ion ligand pillars.<sup>23</sup> In recent years, numerous studies on gas separation systems related to CALF-20 have been published,<sup>24–26</sup> and we have also explored its adsorption properties.<sup>27,28</sup> However, there has been no prior report on CALF-20 for the adsorption of  $\text{NF}_3$  and  $\text{CF}_4$ . This study represents the first investigation into the adsorption and separation performance of CALF-20 for  $\text{NF}_3/\text{CF}_4$ . As a robust adsorbent for  $\text{NF}_3$  capture, CALF-20 demonstrates exceptional structural integrity and cycling stability under various operational conditions (Fig. 1). The temperature-dependent adsorption isotherms (273–313 K) reveal a characteristic Type I physisorption behavior, with  $\text{NF}_3$  uptake capacity increasing systematically from  $32.1 \text{ cm}^3 \text{ g}^{-1}$  at 313 K to  $51.1 \text{ cm}^3 \text{ g}^{-1}$  at 273 K, following expected thermodynamic trends (Fig. 1A). Remarkably, five consecutive adsorption-desorption cycles at 298 K (Fig. 1B) show outstanding reproducibility, with  $\text{NF}_3$  working capacity maintained at  $37.4 \pm 0.7 \text{ cm}^3 \text{ g}^{-1}$  (variation



**Scheme 1** (A) A comparison of some physical parameters of  $\text{NF}_3$  and  $\text{CF}_4$  and the pore structure of CALF-20. (B) The  $\text{NF}_3/\text{CF}_4$  mixture in semiconductor manufacturing is efficiently separated, purified, and recycled through a pressure swing adsorption (PSA) device packed with CALF-20.



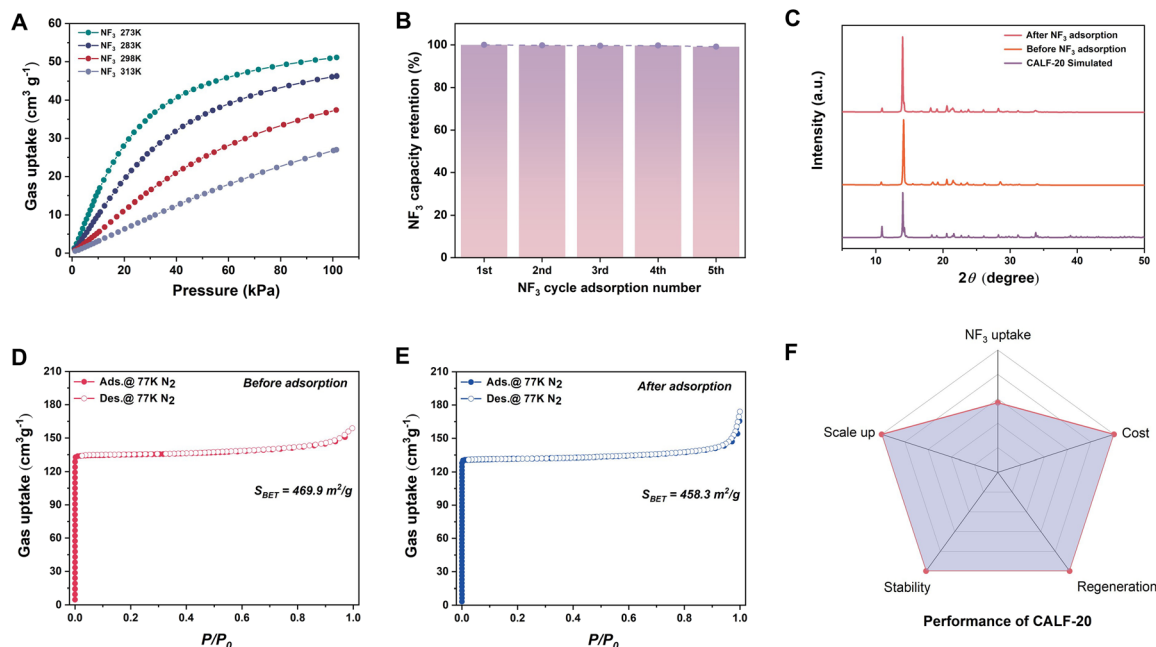


Fig. 1 Adsorption properties and cycling stability of CALF-20 for  $\text{NF}_3$  capture. (A) The  $\text{NF}_3$  adsorption isotherms on CALF-20 at different temperatures. (B) Capacity retention performance of  $\text{NF}_3$  cycle adsorption. (C) The PXRD pattern of CALF-20 before and after  $\text{NF}_3$  adsorption. (D) The  $\text{N}_2$  sorption isotherms at 77 K before  $\text{NF}_3$  adsorption. (E) The  $\text{N}_2$  sorption isotherms at 77 K after  $\text{NF}_3$  adsorption. (F) The five-criteria radar chart of the CALF-20.

<2%), demonstrating excellent cycling stability that meets industrial requirements for long-term operation. Notably, CALF-20 demonstrates exceptional stability toward  $\text{NF}_3$  – a unique characteristic unmatched by other MOF materials. To our knowledge, it represents the first MOF capable of maintaining consistent  $\text{NF}_3$  adsorption performance through multiple cycles without observable performance degradation. Comprehensive characterization further confirms the structural robustness of the framework. The PXRD patterns (Fig. 1C) display identical peak positions and intensities both before and after  $\text{NF}_3$  exposure. There is no observable peak broadening, and no new phases emerge, which indicates that the crystallinity is completely retained.  $\text{N}_2$  physisorption measurements (Fig. 1D and E) show minimal changes in porosity, with BET surface area decreasing only slightly from  $467 \text{ m}^2 \text{ g}^{-1}$  to  $458 \text{ m}^2 \text{ g}^{-1}$  (<2.5% reduction) and pore volume remaining essentially unchanged ( $0.38 \text{ cm}^3 \text{ g}^{-1}$  vs.  $0.37 \text{ cm}^3 \text{ g}^{-1}$ ), suggesting negligible pore damage or structural collapse. These results are supplemented by a five-dimensional performance evaluation (Fig. 1F) that quantitatively assesses the balanced characteristics of CALF-20, including its high  $\text{NF}_3$  uptake capacity (performance), excellent cycling stability (stability), mild regeneration conditions (regeneration), scalable synthesis (cost), and wide operating temperature range (scale up).

The combined evidence from these systematic characterizations establishes CALF-20 as a structurally durable and practically viable adsorbent for industrial  $\text{NF}_3$  separation processes, offering significant advantages over traditional materials in terms of both performance and operational stability. The ability of the material to maintain its adsorption capacity and

structural integrity under repeated cycling, coupled with its temperature-dependent tunability, positions it as a promising candidate for pressure-swing adsorption applications in fluorocarbon purification.

### Molecular sieving for efficient $\text{NF}_3/\text{CF}_4$ separation

CALF-20 exhibited negligible adsorption of  $\text{CF}_4$  across the temperature range of 273–313 K. Adsorption isotherms at 298 K establish CALF-20 as a near-ideal molecular sieve, exhibiting complete exclusion of  $\text{CF}_4$  (uptake  $<1 \text{ cm}^3 \text{ g}^{-1}$ ) while achieving suitable  $\text{NF}_3$  capacity ( $37.4 \text{ cm}^3 \text{ g}^{-1}$  at 100 kPa) (Fig. 2A). Our study reveals that CALF-20 exhibits unique temperature-dependent molecular sieving properties. Across a broad temperature range (273–313 K), the material consistently demonstrates complete exclusion of  $\text{CF}_4$  while maintaining stable  $\text{NF}_3$  uptake (Fig. 2B). A moderate temperature decrease from 298 K to 273 K at 100 kPa does not significantly increase  $\text{CF}_4$  adsorption capacity, but significantly enhances  $\text{NF}_3$  adsorption capacity to  $51.1 \text{ cm}^3 \text{ g}^{-1}$ , representing an increase of approximately 36.6% compared to the uptake at 298 K (Fig. 2C).

CALF-20 exhibits an exceptional  $\text{NF}_3/\text{CF}_4$  adsorption ratio of 41.1 at 298 K (Fig. 2D), significantly surpassing all the previously reported porous materials including ATC-Cu (1.46),<sup>29</sup> HKUST-1 (1.18),<sup>20</sup> Cu(peba)<sub>2</sub> (1.07),<sup>20</sup> Ni(pba)<sub>2</sub> (0.83),<sup>20</sup> Ni-MOF (0.91),<sup>20</sup>  $\text{NH}_2$ -Ni-MOF (1.08),<sup>20</sup>  $\text{Co}_3(\text{HCOO})_6$  (1.03),<sup>30</sup>  $\text{Ni}_3(\text{HCOO})_6$  (1.33),<sup>30</sup>  $\text{Mn}_3(\text{HCOO})_6$  (1.84)<sup>30</sup> and SBMOF-1 (1.16).<sup>31</sup> This outstanding separation performance is of great significance in the field of fluorocarbon separation, as it can potentially revolutionize the industrial separation processes of  $\text{NF}_3/\text{CF}_4$  mixtures, reducing energy consumption and improving separation efficiency. This



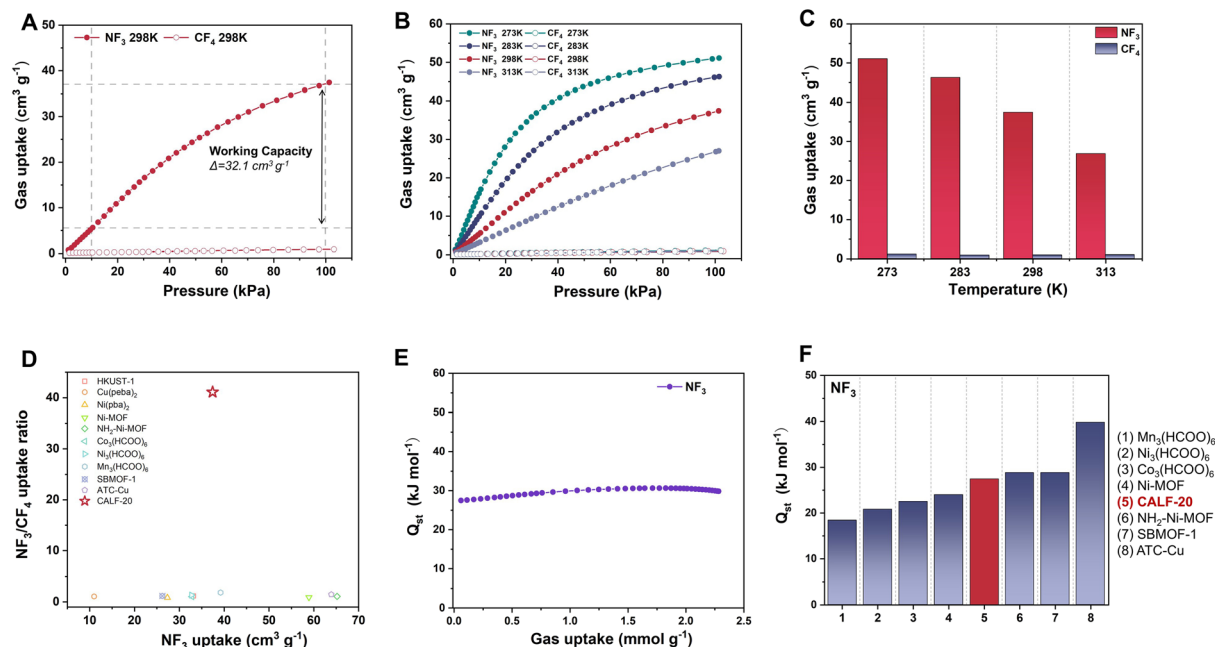


Fig. 2 Molecular sieving and thermodynamic analysis of  $\text{NF}_3/\text{CF}_4$  separation in CALF-20. (A) The  $\text{NF}_3$  and  $\text{CF}_4$  adsorption isotherms of CALF-20 at 298 K. (B) The  $\text{NF}_3$  and  $\text{CF}_4$  adsorption isotherms of CALF-20 at different temperatures. (C) Adsorption capacity of CALF-20 for  $\text{NF}_3$  and  $\text{CF}_4$  at 100 kPa and different temperatures. (D)  $\text{NF}_3$  uptakes and  $\text{NF}_3/\text{CF}_4$  uptake ratio comparison with some reported materials at 298 K and 100 kPa. (E) Isothermic heats of adsorption ( $Q_{\text{st}}$ ) of  $\text{NF}_3$ . (F) The calculated  $\text{NF}_3$   $Q_{\text{st}}$  of CALF-20 and other reported materials.

remarkable enhancement in separation performance demonstrates the unique molecular sieving capability of CALF-20 for  $\text{NF}_3/\text{CF}_4$  mixtures. While other MOFs show adsorption ratios clustered near the vapor–liquid equilibrium prediction ( $\sim 1.25$ ), CALF-20 achieves a 28-fold improvement over the previous best performer (ATC-Cu), establishing new benchmarks for fluorocarbon separations. The superior performance originates from the precisely tuned pore structure of CALF-20. This pore structure enables complete exclusion of  $\text{CF}_4$  while maintaining an effective  $\text{NF}_3$  adsorption capacity. The isothermic heat of adsorption ( $Q_{\text{st}}$ ) for  $\text{NF}_3$  in CALF-20 was determined to be  $27.5 \text{ kJ mol}^{-1}$  at zero coverage (Fig. 2E), calculated from gas adsorption isotherms over 273–313 K. This intermediate binding strength represents an optimal balance for practical applications: sufficiently strong to ensure effective  $\text{NF}_3$  capture at ambient conditions, yet weak enough to permit energy-efficient regeneration (Fig. 2F). Compared with other materials, this unique adsorption energy characteristic endows CALF-20 with distinct advantages in terms of adsorption efficiency and regeneration performance, which is crucial for its large-scale industrial application.

#### Diffusion barriers and host–guest interactions of $\text{NF}_3/\text{CF}_4$ in CALF-20

Minimum energy path (MEP) calculations reveal fundamentally different diffusion mechanisms for  $\text{NF}_3$  and  $\text{CF}_4$  during adsorption in the channels of CALF-20. The energy profile shows that  $\text{NF}_3$  encounters a moderate activation barrier of  $65.6 \text{ kJ mol}^{-1}$  at the channel bottleneck (position-6, Fig. 3A and

B), while  $\text{CF}_4$  faces a substantially higher barrier of  $111.7 \text{ kJ mol}^{-1}$  (position-5, Fig. 3D and E) – consistent with its larger kinetic diameter ( $4.8 \text{ \AA}$  vs.  $4.5 \text{ \AA}$  for  $\text{NF}_3$ ). Furthermore, an analysis of host–guest interaction distances reveals that  $\text{CF}_4$  exhibits stronger interactions ( $\text{H}\cdots\text{F}$ :  $2.60\text{--}3.69 \text{ \AA}$ ) compared to  $\text{NF}_3$  ( $\text{H}\cdots\text{F}$ :  $2.64\text{--}4.03 \text{ \AA}$ ) (Fig. S5), which underscores the steric hindrance associated with its molecular structure.

#### Synergistic analysis of breakthrough experiments and *in situ* infrared spectroscopy

The separation mechanism is synergistically verified by combining the macroscopic separation performance from breakthrough experiments with the microscopic interaction mechanism revealed by *in situ* infrared spectroscopy. In order to evaluate the separation capabilities of CALF-20 for  $\text{NF}_3/\text{CF}_4$  mixtures, we conducted dynamic breakthrough experiments at a temperature of 298 K utilizing an equimolar (50/50, v/v)  $\text{NF}_3/\text{CF}_4$  gas mixture. The gas was introduced at a flow rate of  $6 \text{ mL min}^{-1}$  through a packed column filled with the activated adsorbent. Breakthrough experiments reveal instantaneous  $\text{CF}_4$  permeation (retention time =  $1.3 \text{ min g}^{-1}$ ) versus strong  $\text{NF}_3$  retention ( $5.3 \text{ min g}^{-1}$ ) in CALF-20, demonstrating its molecular sieving selectivity for  $\text{NF}_3/\text{CF}_4$  separations (Fig. 4A). Five consecutive breakthrough cycles demonstrate the stable  $\text{NF}_3/\text{CF}_4$  separation performance of CALF-20. The retention times are nearly identical, which confirms the recyclability of CALF-20 for industrial gas purification (Fig. 4B). Temperature-dependent breakthrough measurements reveal enhanced  $\text{NF}_3/\text{CF}_4$  separation at 273 K and 283 K, with  $\text{NF}_3$  retention time increasing by



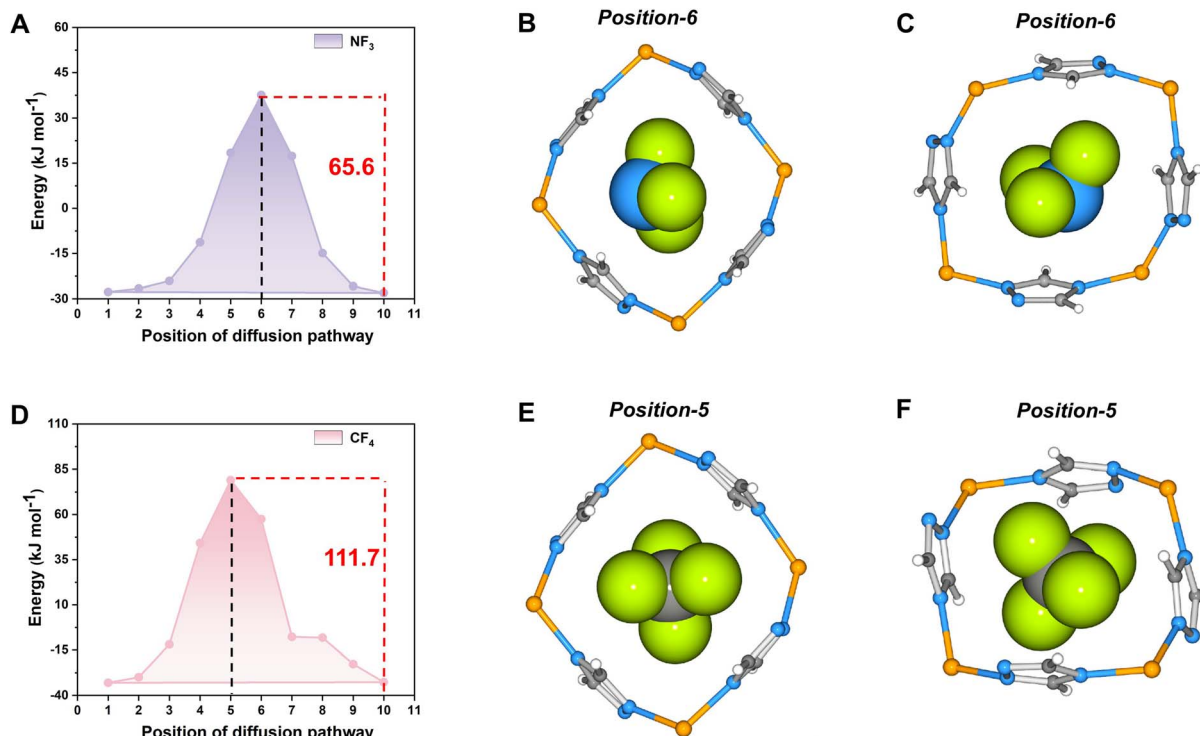


Fig. 3 DFT calculations. Energy profiles for  $\text{NF}_3$  (A) and  $\text{CF}_4$  (D) diffusion in CALF-20; molecular configuration at the positions with maximum energy for  $\text{NF}_3$  (B and C) and  $\text{CF}_4$  (E and F) in CALF-20.

52% and 96% (from 5.3 to 8.1 and 10.2  $\text{min g}^{-1}$ ) while maintaining the instantaneous permeation of  $\text{CF}_4$ , indicating that reducing the temperature appropriately will not significantly

increase energy consumption, but will significantly enhance the separation performance of  $\text{NF}_3/\text{CF}_4$  (Fig. 4C). Regeneration studies at 298 K using He purge gas ( $6 \text{ mL min}^{-1}$ ) revealed

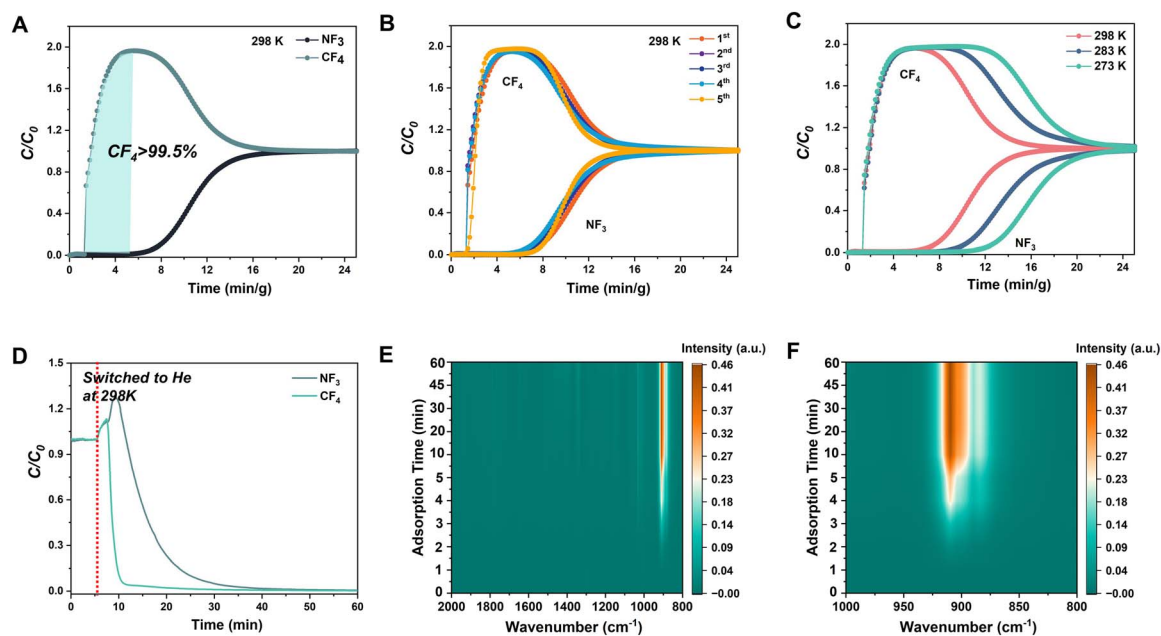


Fig. 4 The breakthrough performance and *in situ* infrared spectroscopy of CALF-20. (A) The  $\text{NF}_3/\text{CF}_4$  breakthrough curve of CALF-20 at 298 K (adsorption condition:  $\text{NF}_3/\text{CF}_4$  v/v 50/50 with the flow rate of  $6 \text{ mL min}^{-1}$ ). (B) Five cycles of column breakthrough experiments. (C) The  $\text{NF}_3/\text{CF}_4$  breakthrough curves of CALF-20 at different temperatures. (D) Desorption curves by He purge with the flow rate of  $6 \text{ mL min}^{-1}$  at 298 K. (E) *In situ* 3D DRIFTS spectral mapping of 1%  $\text{NF}_3$  adsorption on CALF-20 from 0–60 min. (F) *In situ* DRIFTS mapping showing localized N–F bond perturbations ( $910 \text{ cm}^{-1}$ ).



distinct desorption kinetics where  $\text{CF}_4$  was rapidly eluted, while  $\text{NF}_3$  exhibited prolonged retention. This directly demonstrates that CALF-20 had a stronger affinity for  $\text{NF}_3$  at room temperature (Fig. 4D). To investigate the interaction mechanism between  $\text{NF}_3$  and CALF-20, we employed *in situ* FTIR spectrum to monitor real-time vibrational changes during  $\text{NF}_3$  adsorption. Within the 2000–800  $\text{cm}^{-1}$  range, the FTIR spectrum exhibited only the N–F asymmetric stretching vibration of  $\text{NF}_3$  at 910  $\text{cm}^{-1}$  (Fig. 4E). *In situ* FTIR spectroscopy of  $\text{NF}_3$  adsorbed in CALF-20 exhibited an unshifted N–F asymmetric stretching vibration at 910  $\text{cm}^{-1}$  (Fig. 4F), which is identical to the infrared resonance peak reported in the references for pure  $\text{NF}_3$  gas measurements.<sup>32</sup> This observation suggests that the interaction between  $\text{NF}_3$  and CALF-20 is weak and primarily governed by physisorption. Besides, the 3D DRIFTS spectra recorded during desorption (Fig. S6) showed a symmetric decrease in the 910  $\text{cm}^{-1}$  band intensity, mirroring the adsorption profile and confirming the reversibility of  $\text{NF}_3$  uptake—an essential attribute for practical PSA applications. This reversibility, coupled with the sustained framework integrity (no new peaks or shifts in XRD patterns during multiple adsorption–desorption cycles), further underscores the structural stability of CALF-20 under operational conditions.

Combining the different diffusion energy barriers obtained from our DFT calculations (65.6  $\text{kJ mol}^{-1}$  vs. 111.7  $\text{kJ mol}^{-1}$ ) and breakthrough data demonstrating high  $\text{NF}_3/\text{CF}_4$  selectivity, we conclude that molecular sieving in CALF-20 is governed primarily by sieving rather than differential adsorption affinity. The retention of the vibrational signature of  $\text{NF}_3$  further confirms the structural stability of the framework during  $\text{NF}_3$  gas uptake.

## Conclusion

In summary, CALF-20, a metal–organic framework with precisely engineered 4.8 Å pores, has emerged as a breakthrough solution for the separation of nitrogen trifluoride ( $\text{NF}_3$ ) and carbon tetrafluoride ( $\text{CF}_4$ ) in semiconductor manufacturing. This material achieves an  $\text{NF}_3/\text{CF}_4$  uptake ratio of 41.1 and can produce  $\text{CF}_4$  with a purity of >99.5% through breakthrough experiments at 298 K, setting a new benchmark for fluorocarbon separation. The unique pore structure of CALF-20 enables selective molecular sieving of  $\text{NF}_3$  (kinetic diameter: 4.5 Å) while effectively excluding  $\text{CF}_4$  (4.8 Å), as confirmed by structural characterization and computational studies. The remarkable stability and recyclability of the framework over multiple adsorption cycles, combined with its mild regeneration conditions and scalable synthesis, position it as a practical and cost-effective choice for industrial gas purification. This work not only addresses a critical environmental and economic challenge in the semiconductor industry but also provides a model for developing advanced porous materials that can achieve high selectivity and stability for challenging gas separations. By providing a viable way for the energy-efficient recovery of electronic special gases, CALF-20 supports the transition of the semiconductor sector to sustainable practices and the goal of achieving net-zero emissions by 2050.

## Author contributions

Q.-Y. Y. initiated and supervised the research. Q.-Y. Y. and Y.-T. L. designed the project and experiments. Y.-T. L. performed the adsorbents preparation and gas adsorption experiments. L.W.L. and L.X.X performed the simulated calculations. Y.-Y. G., T.-Y. Z. and N. G. performed *in-situ* infrared spectroscopy measurements. Q.-Q. G. provided financial support for the study. L.-P. Z., L. X., S.-M. W., and Q.-Y. Y. discussed the experimental results and provided valuable suggestions. Y.-T. L. wrote the manuscript. Q.-Y. Y. performed manuscript edits and revisions. All authors contribute to the final manuscript and the interpretation of the results.

## Conflicts of interest

There are no conflicts to declare.

## Data availability

Additional details regarding the experimental and calculation data are given in the SI, including *in situ* infrared purging data in Fig. S1–S6 and Table S1 and S2. See DOI: <https://doi.org/10.1039/d5sc04966k>.

## Acknowledgements

Y.-T. L. and W. L. L. contributed equally to this work. This work was financially supported by the National Natural Science Foundation of China (No. 22371221) and the Youth Innovation Promotion Association of the Chinese Academy of Sciences (No. 2021044) and Beijing Nova Program (2024072).

## References

- 1 E. Schmidt, AI, great power competition & national security, *Daedalus*, 2022, **151**, 288–298.
- 2 S. Raoux, T. Tanaka, M. Bhan, H. Ponnkanti, M. Seamons, T. Deacon, L.-Q. Xia, F. Pham, D. Silveti and D. Cheung, Remote microwave plasma source for cleaning chemical vapor deposition chambers: Technology for reducing global warming gas emissions, *J. Vac. Sci. Technol. B*, 1999, **17**, 477–485.
- 3 M. B. Chang and J.-S. Chang, Abatement of PFCs from semiconductor manufacturing processes by nonthermal plasma technologies: A critical review, *Ind. Eng. Chem. Res.*, 2006, **45**, 4101–4109.
- 4 R. Joeri, L. David, C. Brian and R. Keywan, emissions levels required to limit warming to below 2°C, *Nat. Clim. Change*, 2020, **3**, 405–412.
- 5 M. J. Prather and J. Hsu,  $\text{NF}_3$ , the greenhouse gas missing from Kyoto, *Geophys. Res. Lett.*, 2008, **35**, L12810.
- 6 B. A. Wofford, M. W. Jackson, C. Hartz and J. W. Bevan, Surface wave plasma abatement of  $\text{CHF}_3$  and  $\text{CF}_4$  containing semiconductor process emissions, *Environ. Sci. Technol.*, 1999, **33**, 1892–1897.



- 7 H. S. Kim, E. Y. Kim and P. S. Lee, Study of the enrichment of  $\text{NF}_3$  waste gas using zeolite and polymeric membranes, *Sep. Purif. Technol.*, 2019, **220**, 1–7.
- 8 P. Purohit and L. Höglund-Isaksson, Global emissions of fluorinated greenhouse gases 2005–2050 with abatement potentials and costs, *Atmos. Chem. Phys.*, 2017, **17**, 2795–2816.
- 9 K. M. Stanley, D. Say, J. Mühle, C. M. Harth, P. B. Krummel, D. Young, S. J. O'Doherty, P. K. Salameh, P. G. Simmonds and R. F. Weiss, Increase in global emissions of HFC-23 despite near-total expected reductions, *Nat. Commun.*, 2020, **11**, 397.
- 10 C. Y. Chuah, Y. Lee and T.-H. Bae, Potential of adsorbents and membranes for  $\text{SF}_6$  capture and recovery: A review, *Chem. Eng. J.*, 2021, **404**, 126577.
- 11 C.-F. O. Yang, S.-H. Kam, C.-H. Liu, J. Tzou and J.-L. Wang, Assessment of removal efficiency of perfluorocompounds (PFCs) in a semiconductor fabrication plant by gas chromatography, *Chemosphere*, 2009, **76**, 1273–1277.
- 12 S. Singh, F. H. Tezel and P. J. Harlick, Adsorption of tetrafluoromethane and nitrogen by various adsorbents, *Sep. Sci. Technol.*, 2002, **37**, 2763–2784.
- 13 W. Fu, J. Wang, Y. Shi, Y. Li, Z. Sui, L. Wang, Y. Wang and X. Xu, One-step self-activated carbon adsorbent with synergistic micropore-mesopore structure for exceptional  $\text{SF}_6/\text{N}_2$  separation performance, *Carbon*, 2025, **232**, 119839.
- 14 W. Fu, J. Wang, Y. Li, Z. Sui and X. Xu, Investigation on the pore structure-performance relationship of porous carbon adsorbents for  $\text{SF}_6/\text{N}_2$  separation via fine pore modulation, *Sep. Purif. Technol.*, 2024, **348**, 127788.
- 15 Y. Shi, J. Wang, W. Fu, Y. Li, Z. Sui and X. Xu, In-situ activated carbon adsorbents with tailored pore structures for efficient  $\text{SF}_6$  capture and high-purity recovery, *Sep. Purif. Technol.*, 2025, **360**, 130978.
- 16 J. Li, Y. Chen, T. Ke, Y. Jin, R. Fan, G. Xu, L. Yang, Z. Zhang, Z. Bao, Q. Ren and Q. Yang, Efficient continuous  $\text{SF}_6/\text{N}_2$  separation using low-cost and robust metal-organic frameworks composites, *Nat. Commun.*, 2025, **16**, 632.
- 17 S. M. Wang, X. T. Mu, H. R. Liu, S. T. Zheng and Q. Y. Yang, Pore-structure control in metal-organic frameworks (MOFs) for capture of the greenhouse gas  $\text{SF}_6$  with record separation, *Angew. Chem., Int. Ed.*, 2022, **134**, e202207066.
- 18 F. Shahzad, Y. B. Zaied, M. A. Shahzad and F. Mahmood, Insights into the performance of green supply chain in the Chinese semiconductor industry, *Int. J. Prod. Econ.*, 2024, **273**, 109286.
- 19 K. Adil, Y. Belmabkhout, R. S. Pillai, A. Cadiou, P. M. Bhatt, A. H. Assen, G. Maurin and M. Eddaoudi, Gas/vapour separation using ultra-microporous metal-organic frameworks: insights into the structure/separation relationship, *Chem. Soc. Rev.*, 2017, **46**, 3402–3430.
- 20 S.-M. Wang, H.-L. Lan, G.-W. Guan and Q.-Y. Yang, Amino-functionalized microporous MOFs for capturing greenhouse gases  $\text{CF}_4$  and  $\text{NF}_3$  with record selectivity, *ACS Appl. Mater. Interfaces*, 2022, **14**, 40072–40081.
- 21 S.-M. Wang, Q. Zhang, Y.-T. Li, S.-C. Liu and Q.-Y. Yang, Destructive Adsorption of Nitrogen Trifluoride ( $\text{NF}_3$ ) Using M-MOF-74 with Open Metal Sites, *Chem Bio Eng.*, 2024, **1**, 535–540.
- 22 M.-T. Huang and P.-M. Zhai, Achieving Paris Agreement temperature goals requires carbon neutrality by middle century with far-reaching transitions in the whole society, *Adv. Clim. Change Res.*, 2021, **12**, 281–286.
- 23 J.-B. Lin, T. T. Nguyen, R. Vaidhyanathan, J. Burner, J. M. Taylor, H. Durekova, F. Akhtar, R. K. Mah, O. Ghaffari-Nik and S. Marx, A scalable metal-organic framework as a durable physisorbent for carbon dioxide capture, *Science*, 2021, **374**, 1464–1469.
- 24 X. Peng, L. Zhao, Y.-L. Peng, C. Deng, Y. H. Andaloussi, H. Pan, Y.-J. Tian, J.-S. Zou, R. Krishna, B. Liu, C. Deng, P. Xiao, C. Sun, M. J. Zaworotko, G. Chen and Z. Zhang, One-Step Ethylene Purification from a Seven-Component Cracking Gas Mixture with Sorbent-Sorbate Induced-Fit, *CCS Chem.*, 2025, **7**, 1054–1066.
- 25 X. Wang, T. Zhao, Y. Cai, Y. Zheng, Y. Chen and J. Gao, Reversed  $\text{CO}_2/\text{C}_2\text{H}_2$  separation with ultrahigh carbon dioxide adsorption capacity in Zn-based pillared metal-organic frameworks, *J. Solid State Chem.*, 2023, **327**, 124280.
- 26 T. Wu, C. Yu, R. Krishna, Z. Qiu, H. Pan, P. Zhang, X. Suo, L. Yang, X. Cui and H. Xing, Porous materials with suitable pore size and dual-functional sites for benchmark one-step ethylene purification, *AIChE J.*, 2024, **70**, e18312.
- 27 Y.-T. Li, W. Li, L.-P. Zhang, L. Xu, S. Ni, Y. Jiang, X. Li and Q.-Y. Yang, Zinc-Based flexible coordination network for precise butane isomer sieving and low-carbon alkane recovery from oilfield associated gas, *Sep. Purif. Technol.*, 2025, **363**, 132018.
- 28 Y. T. Li, W. Li, L. P. Zhang, S. Ni, Y. Jiang, X. Li and Q. Y. Yang, Wide Temperature Sieving of n-Butene and iso-Butene by a Zinc-Based Coordination Network with Record Separation, *Adv. Funct. Mater.*, 2025, **35**, 2411951.
- 29 Z.-W. Fan, Y. Wang, J. Liu, Z.-T. Cheng, C. Wang and Z. Niu, Metal-Organic Framework-Based  $\text{NF}_3$  Nanotrap for the Separation of  $\text{NF}_3$  and  $\text{CF}_4$ , *ACS Appl. Mater. Interfaces*, 2024, **17**, 2349–2354.
- 30 Y. Wu, T. Yan, W. Zhang, S. Chen, Y. Fu, Z. Zhang and H. Ma, Adsorption interface-induced  $\text{H}\cdots\text{F}$  charge transfer in ultramicroporous metal-organic frameworks for perfluorinated gas separation, *Ind. Eng. Chem. Res.*, 2022, **61**, 13603–13611.
- 31 Y. Wu, S. Wang, W. Zhang, S. Chen, Z. Zhang, B. Yang, S. Li and H. Ma, Enhancing perfluorinated electron specialty gases separation selectivity in ultra-microporous metal organic framework, *Sep. Purif. Technol.*, 2022, **289**, 120739.
- 32 A. Guber and U. Köhler, FTIR spectroscopy for the analysis of selected exhaust gas flows in silicon technology, *J. Mol. Struct.*, 1995, **348**, 209–212.

